AN EXPERIMENTAL STUDY ON HYDRATION OF VARIOUS MAGNESIA RAW MATERIALS

[#]ILONA JASTRZĘBSKA , JACEK SZCZERBA, RYSZARD PROROK, EDYTA ŚNIEŻEK

AGH University of Science and Technology, Faculty of Materials Science and Engineering,
Department of Ceramics and Refractories, al. Mickiewicza 30, 30-059 Kraków, Poland

[#]E-mail: ijastrz@agh.edu.pl

Hydration of various commercially available magnesia raw materials were studied under hydrothermal conditions. Raw materials were characterized by XRD, XRF, TG/DTA and SEM/EDS methods. Subsequently, they were subjected to hydration test conducted at temperature of 162°C and presuure of 552 kPa according to ASTM C 554-92 standard. The evolution of phase, microstructure and physicochemical behaviour after hydration test were analysed by XRD, DTA/TG and SEM/EDS. The results showed that presence of the specific secondary phases plays a crucial role in preventing MgO grains against the hydration. Merwinite, monticellite, magnesioferrite and srebrnodolskite were found to constitute protector-like phases that inibit hydration process of magnesia.

INTRODUCTION

Magnesia raw materials are materials currently essential for the production both shaped and unshaped refractories finding the application in the steel industry. Although MgO exhibits numerous advantages, such as a high melting point of 2825°C, basic slag and corrosion resistance, it is susceptible to react with water. This reaction results in the formation of brucite Mg(OH)$_2$ according to Equation 1 [1-3].

$$MgO + H_2O_{(liquid\ or\ water\ vapor)} = Mg(OH)_2 \qquad (1)$$
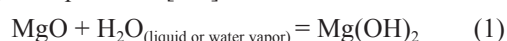
The hydration reaction of periclase can take place during long transport of magnesia from remote countries. It may also occur during storage of the material as well as mixing with water or curing of the castable mixture [3-7]. Time and high humidity promote the MgO hydration reaction greatly which results in a large volumetric expansion due to the fact that the density of formed brucite Mg(OH)$_2$ is by 33 % lower than the density of periclase MgO. The increase of volume leads to the tensile and compressing stresses formation what results in cracks and subsequent damage of the material [3, 4, 6, 8, 9, 10, 12]. Therefore it is worth to draw attention to the problem of MgO hydration because it may affect the quality of the final product containing MgO considerably. According to the literature [9, 11] there are a few factors that influence magnesia hydration reaction. These are chemical and phase composition of magnesia raw materials, size and crystallographic orientation of the MgO crystals, temperature of environment as well as relative humidity and time. The higher temperature, time and pressure of water vapour, the higher the hydration rate. Moreover, the smaller crystal sizes, higher specific surface area and pore volume of the oxide particles, the easier and faster hydration reaction.

It is reported that the hydration mechanism of MgO in contact with liquid water differs from that with water vapour. Braun and Feitknecht described the mechanism of the MgO hydration reaction with water vapour as a multistep process which proceeds stepwise [13, 1]:

a) physical adsorption of water vapour on the surface of MgO crystal and formation of a layer of liquid water,

b) chemical reaction between water molecules and MgO resulting in a formation of a thin layer of Mg(OH)$_2$,

c) Mg(OH)$_2$ dissolution in the water layer,

d) supersaturation of the water layer with Mg^{2+} and OH$^-$ ions and subsequent crystallization of Mg(OH)$_2$.

On the other hand, the mechanism of MgO hydration with liquid water consists of three primary steps, as suggested by Rocha et al. [14], which are as follows:

a) adsorption of water on the surface of MgO and its simultaneous diffusion through the pores inside the MgO grains,

b) dissolution of MgO by the absorbed water and a related change of porosity,

c) supersaturation of water with Mg^{2+} and OH$^-$ ions leading to nucleation and growth of Mg(OH)$_2$ on the MgO crystals surface.

The reaction velocity in liquid water and water vapour environment increases with temperature. It was reported [7] that, a 10°C rise in temperature induces the increase in hydration velocity by around 60 %.

Magnesia raw materials contain besides MgO also some amount of the impurities, such as SiO_2, CaO, Al_2O_3, Fe_2O_3 oxides. Depending on the CaO/SiO_2 ratio these residual oxides react with each other to form different secondary phases that coexist with MgO in the material. Among these phases there can occur forsterite Ma_2SiO_4, merwinite $Ca_3MgSi_2O_8$, monticellite $CaMgSiO_4$, belite Ca_2SiO_4, alite Ca_3SiO_5, spinel $MgAl_2O_4$, magnesium ferrite $MgFe_2O_4$, srebrnodolskite $Ca_2Fe_2O_5$, brownmilleryte Ca_2AlFeO_5 and calcium oxide CaO (Table 1). Their vulnerability to reaction with water differs from each other. Phases such as forsterite, merwinite and monticellite are less susceptible to hydration. On the other hand, calcium silicate phases like Ca_2SiO_4 and Ca_3SiO_5 react with water easier forming the C–S–H phase [11, 15].

When the molar ratio of CaO/SiO_2 is > 2 and Al_2O_3/Fe_2O_3 < 1, then ferrite phases appear in the microstructure of magnesia raw material. On the other hand, when the molar ratio of Al_2O_3/Fe_2O_3 is > 1 then calcium aluminates coexist with MgO, Ca_2SiO_4 and Ca_2AlFeO_5 in the microstructure of the material. It is known that aluminate phases react with water, forming C-A-H hydrates with different stoichiometry which crystallize into needle-like crystals [13, 15].

Bearing this in mind, the aim of this article is to clarify the influence of different secondary phases coexisting with MgO and an exposure to hydrothermal environment on the hydration behaviour of various magnesia raw materials. This will be evaluated by measuring hydration rate according to ASTM C 544-92 [5,16] and subsequent precise analysis of the microstructure by XRD, DTA/TG, BSE-SEM/EDS.

EXPERIMENTAL

Three kinds of sintered magnesia raw materials (designated as K1, K2, K3) and one type of fused magnesia (designated as F) were selected for the investigation.

Study on various magnesia raw materials were divided into three steps as it is shown in Table 2.

Chemical composition of the samples was determined by XRF technique (using Philips X'Unique II spectrometer). X-ray diffraction (XRD; FPM Seifert XRD7) was performed using Cu K_α radiation. The powder samples were tested in the 5 - 90 2θ degrees range. Thermal analysis was conducted using the TG/DTA analyzer (SDT 2960 TA INSTRUMENTS) in the range of temperatures 20 - 1000°C under the air atmosphere and with the heating rate of 10°C·min^{-1}. The test samples were also subjected to BSE-SEM/EDS microstructure analysis with the use of Nova Nanosem 300.

The hydration tests of four magnesia raw materials

Table 1. Phases coexisting with periclase in the magnesia refractories in dependence on CaO/SiO_2 ratio [15].

CaO/SiO_2 molar ratio	Silicate phases	Residual phases
0	forsterite M_2S - $2MgO·SiO_2$	MA[a], MF[b]
0 – 1	M_2S, CMS	MA[a], MF[b]
1	monticellite CMS-$CaO·MgO·SiO_2$	MA[a], MF[b]
1 – 1.5	CMS, C_3MS_2	MA[a], MF[b]
1.5	merwinite C_3MS_2 - $3CaO·MgO·2SiO_2$	MA[a], MF[b]
1.5 – 2	C_3MS_2, C_2S	MA[a], MF[b]
2	dicalcium silicate C_2S - $2CaO·SiO_2$	C_4AF[c], MA[a], MF[b]
2 – 3	C_2S, C_3S	C_4AF[c], C_2F[d] (A/F < 1)
3	tricalcium silicate C_3S - $3CaO·SiO_2$	C_4AF[c], C_2F[d] (A/F < 1)
> 3	C_3S, CaO	C_4AF[c], C_2F[d] (A/F < 1)

[a] MA – magnesium aluminium spinel $MgO·Al_2O_3$,

[b] MF – magnesium iron spinel $MgO·Fe_2O_3$,

[c] C_4AF – tetracalcium aluminoferrite $4CaO·Al_2O_3·Fe_2O_3$, d C_2F – dicalcium ferrite $2CaO·Fe_2O_3$

Table 2. Examination procedure of magnesia raw materials.

Before-hydration examinations	Hydration test	After-hydration examinations
XRD, XRF	Test in autoclave acc. to ASTM-C544.	XRD, XRF
DTA/TG	Examination conditions:	DTA/TG
BSE-SEM/EDS	T = 162°C, p = 552 kPa, t = 5 h	BSE-SEM/EDS

(K1, K2, K3, F) were carried out in accordance with ASTM C 544-92 standard under severe conditions of water va-pour pressure of 552 kPa and at elevated temperature of 162°C. The test sample consisted of equal weight parts of three different fractions (3.35 - 1.70 mm, 1.7 - 0.850 mm and 0.850 - 0.425 mm) to obtain the total weight of the sample 100 g. After mixing and placing the sample in a crucible it was dried to constant weight at 110°C. Then it was put into the autoclave and maintained under hydrothermal conditions for 5 hours. After-hydration samples were dried to constant weight, and then weighed. Subsequently, they were sieved through 0.3 mm sieve to divide them into a fine fraction – henceforth referred as "*F*" (passed through the sieve) and a coarse referred as "*C*" (retained on the sieve). This retained fraction was weighed. The rate of MgO hydration was calculated as stated in Equation 2:

$$hydration\ rate\ [\%] = (G - H)/G \cdot 100 \quad (2)\ [16]$$

where, *G* is weight of the dried sample after hydration; *H* is weight of the hydrated sample retained on the 0.3 mm sieve. The weight percentage of material that passed through the 0.3 mm sieve after hydration test was an indicator of hydration rate. The average hydration rate for each sample was accounted for by the average value from three measurements.

The phase composition evolution on after-hydration samples was determined by XRD (both *F* and *C* fractions), DTA/TG (*F* fractions). The microstructures of all the polished section surfaces of magnesia *C* samples were observed using a scanning electron microscope (Nova Nanosem 300) equipped with an energy dispersive spectrometer (EDS) operated at 18 kV. Microscopic observations were performed using BSE mode.

RESULTS AND DISCUSSION

Before-hydration examinations – characterization of the test materials

Chemical, phase composition and microstructure analysis (XRF, XRD, SEM)

Chemical composition results obtained using XRF method are shown in the Table 3. The K3 sample possesses the highest amount of iron oxide exceeding 7 wt. %, the highest CaO/SiO$_2$ molar ratio and simuntaneously

Table 3. Characterization of the raw materials tested.

Sample	Oxide content, wt. %					CaO/SiO$_2$ molar ratio	Source
	MgO	CaO	SiO$_2$	Al$_2$O$_3$	Fe$_2$O$_3$		
K1	96.4	2.31	0.65	0.18	0.17	3.8	Australia
K2	95.0	1.66	1.76	0.58	0.75	1.0	China
K3	87.53	3.25	0.56	0.29	7.56	6.2	Slovakia
F	98.0	0.97	0.38	0.12	0.48	2.7	China

it has the lowest amount of main component MgO. K1 magnesia is characterized by the lowest level of impurities in the form of iron oxide. Fused magnesia (F) is the purest raw material containing the highest amount of MgO equaled 98 wt. %.

Phase composition of magnesia samples, as determined by the XRD analysis, is given in Figure 1 for K1, K2, K3 and F, respectively. All the diffraction patterns reveal test samples having predominantly MgO (designated as 'M' in the XRD spectra). Moreover, additional low-intensity XRD peaks, indicated as black dots in Figure 2 and lying in the 2θ range of 24 ÷ 36°, can also be seen in all the spectra what indicate presence of secondary phases. Table 4 shows experimental patterns of MgO and secondary phases as well as referred peaks taken from ICDD crystallographic database. Sharp peaks for MgO indicate high crystallinity of this phase and 2 theta positions are well agreeable with the referred ones. Low-intensity patterns for secondary phases allow to assume Ca$_2$SiO$_4$ in K1, CaMgSiO$_4$ in K2, MgFe$_2$O$_4$ and Ca$_2$Fe$_2$O$_5$ in K3 and Ca$_3$Mg(SiO$_4$)$_2$ in F sample. These phases were also found during SEM observations as it is depicted in Figure 3. SEM images show differences in amount and distribution of MgO crystals as well as the type and distribution of secondary phases. MgO crystal constitute a dark grey areas while secondary phases are visible as bright areas surrounding magnesia crystals. It can be observed that secondary phases surround the MgO crystals especially in the case of small-crystalline K3 magnesia in which srebrnodolskite Ca$_2$Fe$_2$O$_5$ fills spaces between crystals tightly. Additionally, inside MgO
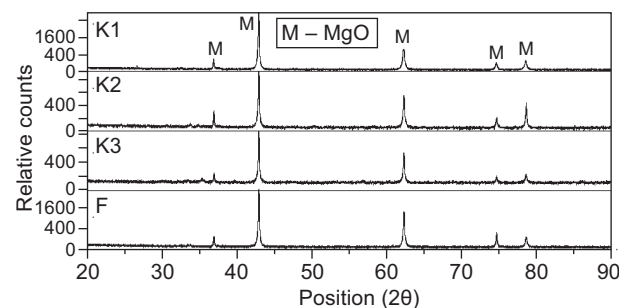
Figure 1. XRD patterns of before-hydration magnesia samples K1, K2, K3, F.
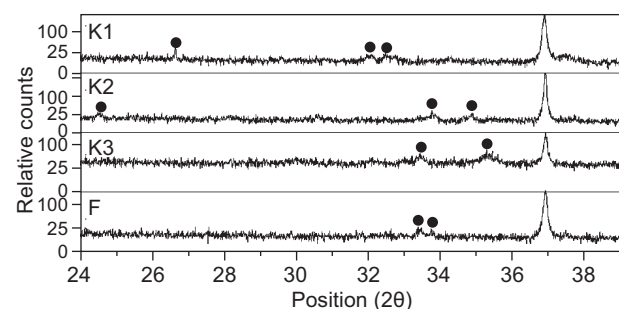
Figure 2. XRD patterns of before-hydration magnesia samples K1, K2, K3, F in the range of 2θ 24 - 39°.

crystals of K3 sample magnesium ferrite $MgFe_2O_4$ is present in the form of bright inclusions. Fused magnesia was found to possess the largest crystals with their size reaching 800 µm. On the other hand, K3 magnesia has the smallest crystals sizes of average 50 µm.

Thermal behaviour – DTA/TG analysis

TG curves of before-hydration magnesia samples depicted in Figure 4 a, b, c, d show small weight decrease approximately 0.2 wt. % in the range of temperatures between 250 and 400°C which can be ascribed to 'primary' brucite decomposition that was formed as a result of water vapour exposure during its storage.

Different temperatures range of brucite decompo-

sition for the test samples indicates that it was differently releasing probably because of variation in the structure, atoms distribution as well as depth from which it was released. At lower temperatures below 200°C the loss of weight is caused by release of free water absorbed on the MgO grains. At the temperatures of 650°C, 620°C, 660°C for K1, K3, F, respectively, a small decline of weight comes from $MgCO_3$ decomposition. Thermogravimetric for K3 magnesia at the temperature above 800°C shows an increase in weight which can be attributed to an oxidation of Fe^{2+} to Fe^{3+} because this sample could contain a residual amount of iron oxide of 2+ valency in the form of siderite $FeCO_3$ or ankerite $CaFe(CO_3)_2$ occurring in the Slovakian magnesia ore from which K3 magnesia was produced [17].
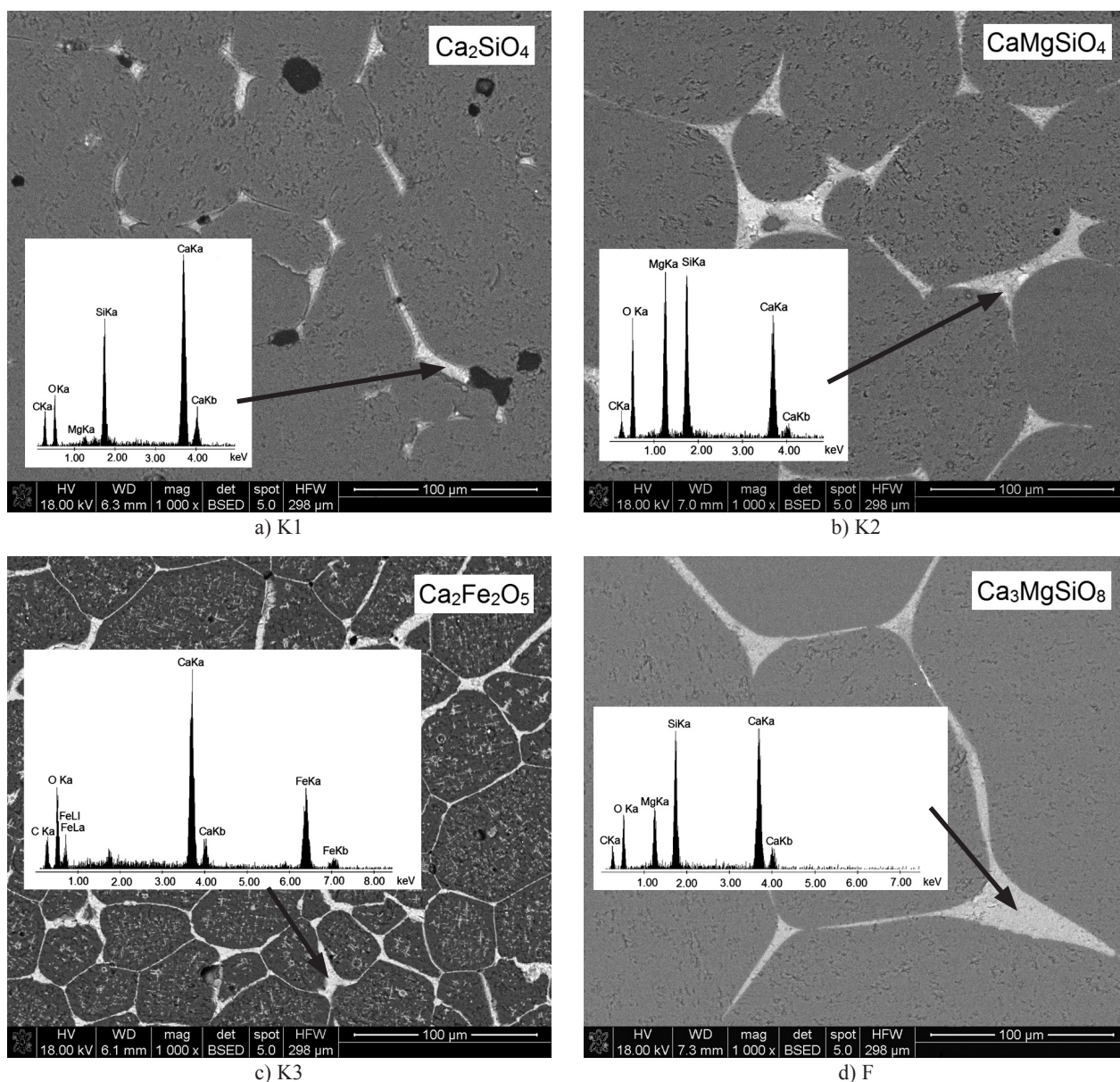
Figure 3. BSE-SEM images with EDS analysis of the test magnesia samples corresponding to different secondary phases present: a) K1, b) K2, c) K3, d) F (magnitude 1000 ×).

Table 4. 2θ positions of the test magnesia samples and referred peaks from JCPDS cards.

Sample designation	2θ (°) for MgO in the test sample	2θ (°) for referred MgO from JCPDS with relative intensity (a.u.)	Additional reflexes	
			2θ (°) in the test sample	2θ (°) for referred phase from JCPDS with relative intensity (a.u.)
K1	36.883	36.862 (11.6)	32.568	32.533 (85)
	42.878	42.824 (100)	32.055	32.078 (100)
	62.230	62.167 (45)	26.637	26.033 (12)
	74.599	74.515 (5.0)		
	78.527	78.4343 (11.1)		
JCPDS/phase	–	01-075-0447/MgO	–	00-031-0299/Ca_2SiO_4
K2	36.911	36.898 (11.6)	33.765	33.898 (100)
	42.877	42.867 (100)	34.841	34.895 (62.8)
	62.267	62.233 (45.1)	24.555	24.644 (69.0)
	74.650	74.598 (5.0)		
	78.599	78.532 (11.1)		
JCPDS/phase	–	01-087-0651/MgO	–	01-084-1323/$CaMgSiO_4$
K3	36.916	36.898 (11.6)	35.314	35.421 (100)[1]
	42.891	42.867 (100)	33.393	33.409 (100)[2]
	62.265	62.233 (45.1)		
	74.643	74.598 (5.0)		
	78.572	78.532 (11.1)		
JCPDS/phase	–	01-087-0651/MgO	–	[1]01-088-1941/$MgFe_2O_4$ [2]01-071-2264/$Ca_2Fe_2O_5$
F	36.912	36.937 (4.0)	33.427	33.409 (100)
	42.899	42.917 (100)	33.742	33.568 (60.2)
	62.269	62.304 (39)		
	74.656	74.691 (5.0)		
	78.579	78.630 (10)		
JCPDS/phase	–	00-045-0946/MgO	–	01-074-382/Ca_3MgSiO_8

Hydration test results

Hydration test results (Table 5) revealed that K1 magnesia possessed the highest hydration susceptibility among all the magnesia raw materials tested. The hydration rate of it is 70.4 % whereas for the rest of the samples it is 36.7 % for K2, 16.5 % for F and 8.4 % for K3. The K1 sample has the molar ratio of CaO/SiO_2 > 2 and also the molar ratio of Al_2O_3/Fe_2O_3 > 1, what leads to specific phases contained in the microstructure, such as calcium silicates (Table 4, Figure 3a), which are well-known to be highly susceptible to hydration [18].

The K3 magnesia sample which reached the lowest hydration rate of 8.4 % (8 times lower than K1) has high

molar ratio of CaO/SiO_2 > 2 but low Al_2O_3/Fe_2O_3 < 1. It contains residual ferrite phases (Tables 1 and 4, Figure 3c) which do not react with water easily and constitute protector-like components of the microstructure. Fused magnesia is naturally resistant to hydration because of its large crystals (Figure 3d) and therefore lower specific surface area, resulted from a high temperature treatment during production of this raw material. As it can be observed from the Table 5 K1 sample exhibits the highest increase of weight after hydration as well as the lowest amount of the coarse fraction. What is worth to emphasize is that in spite of similar total weight of the after-hydration K2, K3 and F samples the amount of C fraction in these samples

Table 5. Hydration test results of the K1, K2, K3, F magnesia samples.

Sample	Average total weight of the sample after hydration (g)	Average weight of the coarse fraction (C) after hydration (g)	Average hydration rate (%)	CaO/SiO_2 mol. ratio	Al_2O_3/Fe_2O_3 mol. ratio	CaO/Al_2O_3 mol. ratio
K1	105.00	31.03	70.4	3.8	1.7	12.8
K2	103.20	65.28	36.7	1.0	1.2	2.9
K3	102.62	93.99	8.4	6.2	0.04	11.2
F	102.27	85.44	16.5	2.7	0.4	8.1
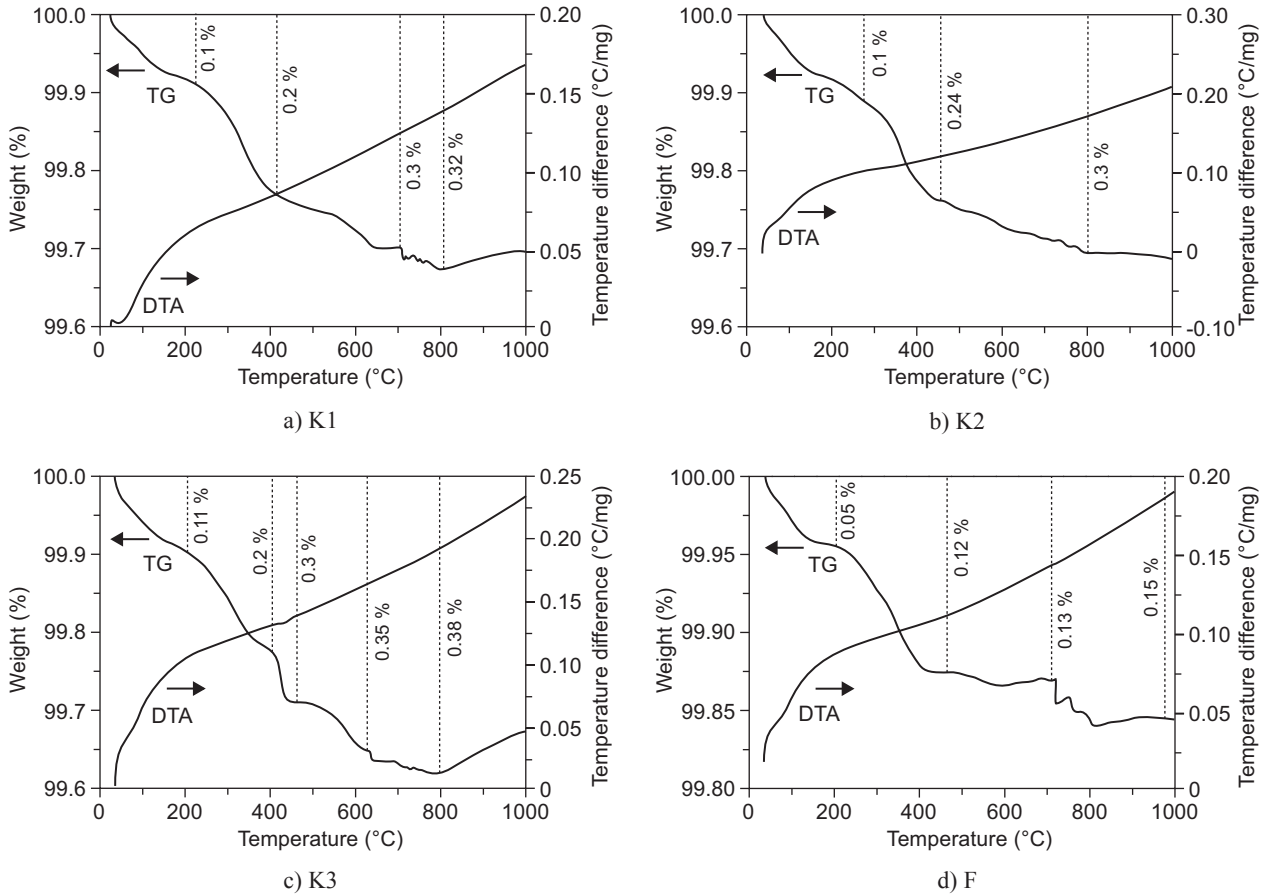
Figure 4. DTA/TG curves of before-hydration magnesia samples a) K1, b) K2, c) K3, d) F.
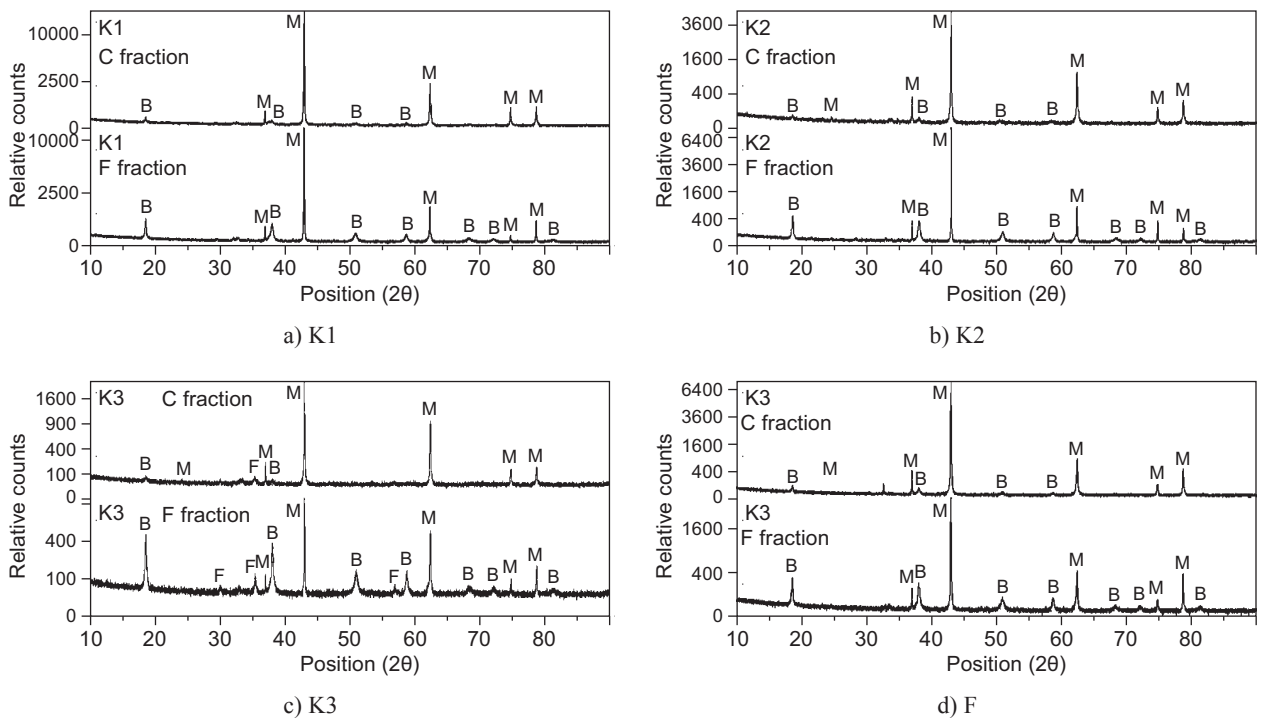
Figure 5. XRD patterns of after-hydration test magnesia samples a) K1, b) K2, c) K3, d) F (C – coarse fraction, F – fine fraction).

is completely different resulting in obtaining different hydration rates. It can be seen that, weight of the C fraction for K3 magnesia has the highest value what explains the lowest vulnerability of this type of magnesia to hydration.

After-hydration examinations
Phase composition - X-Ray Diffraction

Both the fine fraction (F) and the coarse fraction (C) contains 'secondary brucite' in the phase composition (Figure 5), which indicates that hydration of MgO occurred as a result of water vapour exposure during the test in the autoclave. In every XRD pattern for F fraction there is a higher number of peaks related to $Mg(OH)_2$ than for C fraction what justify higher brucite content in the F fraction. This is confirmed by the fact that the fine fraction is the fraction which was crushed and therefore 'produced' as a result of hydration. It can be seen that patterns for $Mg(OH)_2$ phase are not as sharp as those for MgO what can be the result of low a crystallinity or a

solid solution formation.

The XRD diffractogram for K3 samples (Figure 5c) reveals higher-intensity peaks ascribed to magnesium ferrite in comparison to before-hydration sample. This evidences that $MgFe_2O_4$ phase did not undergo chemical changes in the environment of water vapour and is resistant to hydration.

Table 6 shows the 2θ positions for MgO and $Mg(OH)_2$ before and after hydration. The important information is that the environment of water vapour influenced a structure of periclase. It has been observed that 2θ angle for MgO increases after hydration in the coarse fraction of all the magnesia samples. Such a change in the XRD parameters can indicate a decrease of the lattice parameter and shrinkage of the magnesia unit cell. In the fine fraction of K1 and F sample 2θ for MgO generally decreases in relation to coarse fraction but is never lower than the starting value (before hydration). In the case of K2 and K3 samples more peaks for MgO have higher value of 2θ angle in the fine fraction than in the coarse one. If we consider peaks positions for $Mg(OH)_2$ it

Table 6. Changes in 2θ positions for MgO and $Mg(OH)_2$.

	2θ for MgO before hydration	2θ for MgO after hydration		2θ for $Mg(OH)_2$ after hydration	
		C fraction	F fraction	C fraction	F fraction
K1	36.8826	36.9096	36.9002	18.5644	18.5679
	42.8781	42.9001	42.8851	–	32.8033
	62.2303	62.2751	62.2321	37.9716	37.9787
	74.5999	74.6246	74.6171	50.7785	50.8125
	78.5274	78.5868	78.5535	58.5994	58.6062
				–	68.2128
				–	72.0074
				–	81.2634
K2	36.9110	36.9462	36.9588	18.5913	18.5972
	42.8769	42.8769	42.9499	–	32.8784
	62.2666	62.3036	62.2999	37.9934	38.0274
	74.6501	74.6896	74.7050	–	50.8711
	78.5999	78.6245	78.6427	–	58.6681
				–	62.2999
				–	68.2878
				–	72.0761
				–	81.2104
K3	36.9156	36.9363	36.9411	18.5751	18.5646
	42.8909	42.9163	42.9037	38.0303	38.0160
	62.2647	62.2934	62.2932	–	50.8638
	74.6432	74.6599	74.6881	–	58.6534
	78.5721	78.6014	78.6070	–	68.2742
				–	72.0339
				–	81.1408
F	36.9120	36.9448	36.9321	18.5697	18.5726
	42.8990	42.9192	42.9161	32.5946	32.8773
	62.2689	62.2973	62.2906	37.9940	38.0038
	74.6560	74.6755	74.6794	50.8272	50.8487
	78.5799	78.6174	78.6044	58.6264	58.6304
				–	68.1942
				–	72.0171
				–	81.1149

is clearly seen that F fraction of the K1, K2 and F samples characterizes by the higher values of 2θ in comparison to C fraction. The contrasting behavior was observed for the K3 magnesia containing the highest amount of impurities in which 2θ for 'secondary' brucite in the fine fraction were higher with respect to 2θ in the coarse one. A decline in 2θ for C fraction can indicate an incease in lattice parameter and resulting expansion of the unit cell by solid solutions formation. A decrease of 2θ positions in this case can be attributed to incorporation of iron ions in the crystal lattice of magnesium hydroxide, depending on the ionic radii of the reacting species ($Fe^{2+} = 0.074$ nm, $Fe^{3+} = 0.064$ nm, $Mg^{2+} = 0.055$ nm). It is predictable that there are solid solutions between $Ca_2Fe_2O_5$ or $MgFe_2O_4$ and $Mg(OH)_2$, where magnesium ions sites are occupied by iron ions. The knowledge about brucite solid solutions is still thrifty in the literature and will be investigated in the future work.

Thermal behaviour - DTA/TG analysis

Figure 6 displays curves from DTA and TG measurements for the fine fractions (F) obtained after hydration of all the magnesia samples. The first small weight loss to around 200°C for all the samples can be related to free moisture release. A small endothermic band in the case of K1, K2 and F can be observed at temperature around 220°C that can be related to the first stage of crystalline water release from hydromagnesite previously stated by Todor [19]. Hydromagnesite $Mg_5(CO_3)_4(OH)_2 \cdot 4H_2O$ decomposes endothermically over a temperature range of approxi-mately 220 - 640°C in three stage process. The second stage of decomposition occurs around 400°C, and it predictably overlaps with the strong endothermic event with the maximum at about 390°C which we attributed to dehydroxylation of brucite. The loss of weight in the range of 450 - 650°C, shown by TG curve, can be attributed to carbdioxide release from carbonate structure. The correspondence of the endotherm at about 390°C to brucite decomposition was confirmed by the presence of reflexes characteristic for $Mg(OH)_2$ in fine fraction during XRD analysis (Figure 5a, b, c, d).

It can be observed from thermogravimetrics that the weight loss due to brucite decomposition for the K2 and F samples is similar of about 10.5 %. In contrast, for the K1 magnesia it is 7 % and for K3 – 15.5 %.
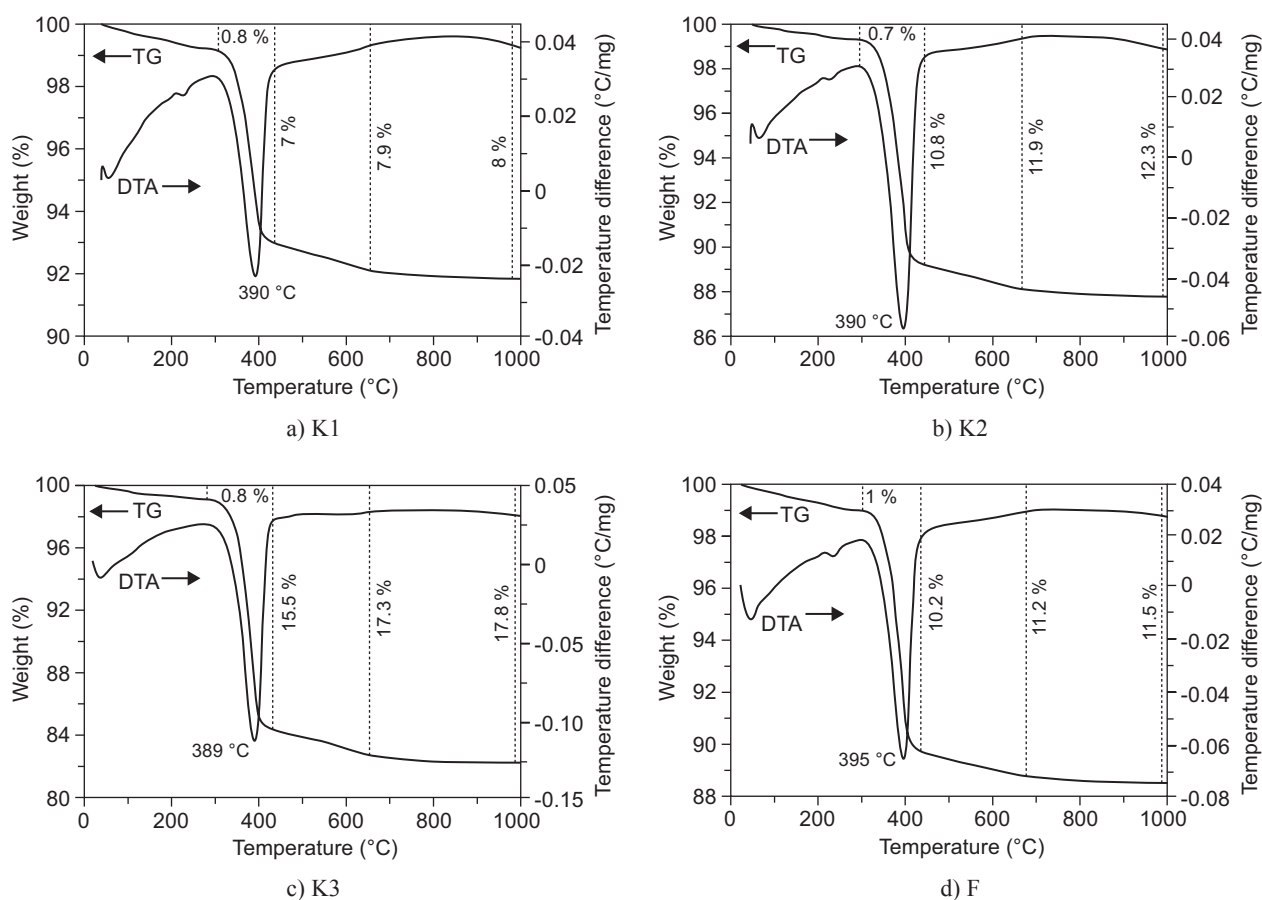
Figure 6. DTA and TG curves for fine fraction (F) of after-hydration magnesia samples a) K1, b) K2, c) K3, d) F.

Microstructure after hydration –
BSE-SEM/EDS analysis

Figure 7 depicts the microstructure of K1 magnesia after hydration in the autoclave. The black continuous area consists of epoxy resin which was utilized to prepare all the samples for the SEM observations. The MgO crystals are clearly visible in the SEM images as bright-gray areas separated from one another by darker grain boundaries. On the rim of the MgO grain (Figure 7a) a dark-gray layer of brucite is spread. Its composition was confirmed by the XRD, TG/DTA measurements. The average thickness of the brucite layer is around 10 μm. Moreover, on the surface of the MgO crystals numerous microcracks are present. They constitute areas more

susceptible to hydration, thus posing an easier reaction path because water penetrates into them more easily and reaches volume of the grain faster (Figure 7b). The mechanism of MgO hydration can be described based on these two images. The hydration reaction initiates on the surface of the MgO grain first (Figure 7a) and subsequently water penetrates the polycrystal resulting in its crushing and formation of many monocrystals. After that the reaction proceeds inside an each individual MgO core (Figure 7b).

The K2 magnesia crystals displayed in Figure 8a,b are oval and 'well-wetted' by monticellite $CaMgSiO_4$ located at the grain boundaries (Figure 8a) and visible as light grey areas. It can be deduced that this 'wetting'
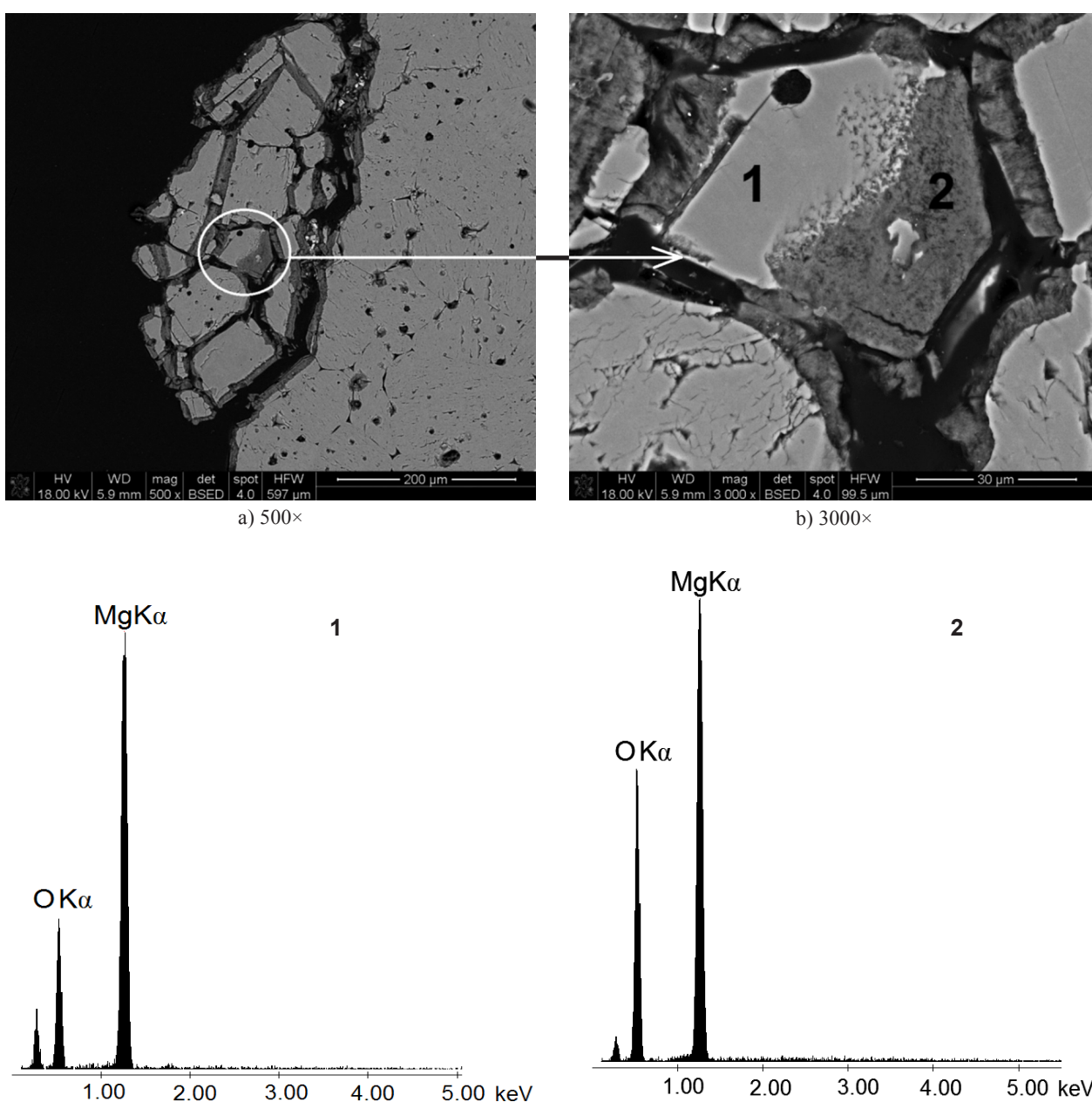
a) 500×

b) 3000×

Figure 7. BSE-SEM images with EDS analysis of the after-hydration K1 magnesia cross-sections (C fraction), in magnitude a) 500 ×, b) 3000 ×.
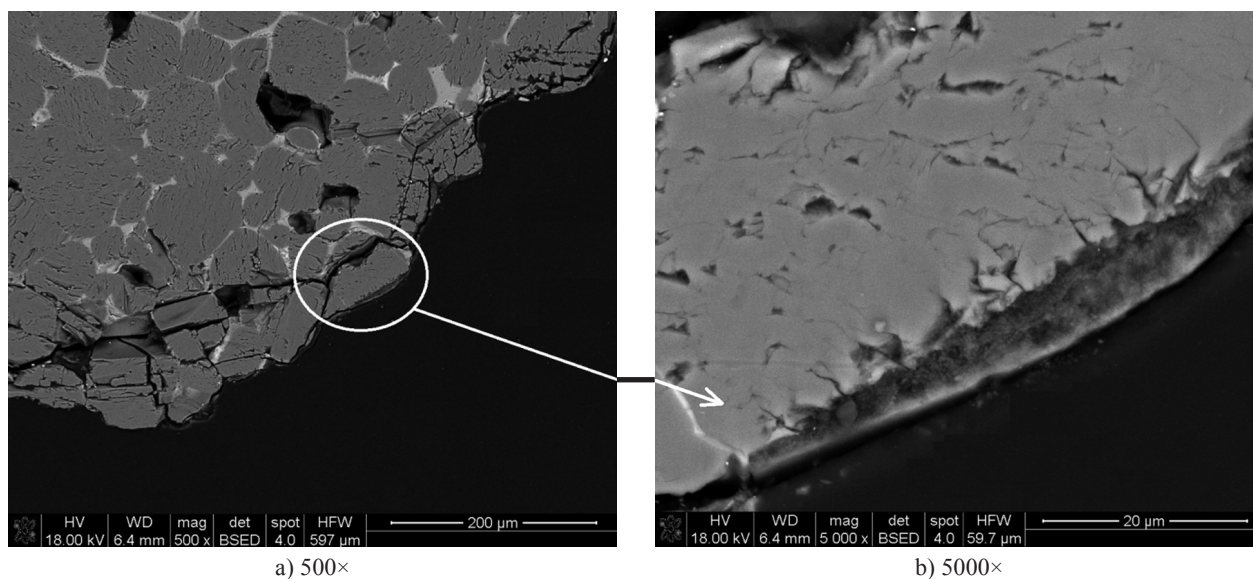
a) 500×   b) 5000×

Figure 8. BSE-SEM images of the after-hydration K2 cross-sections (C fraction), in magnitude a) 500 ×, b) 5000 ×.
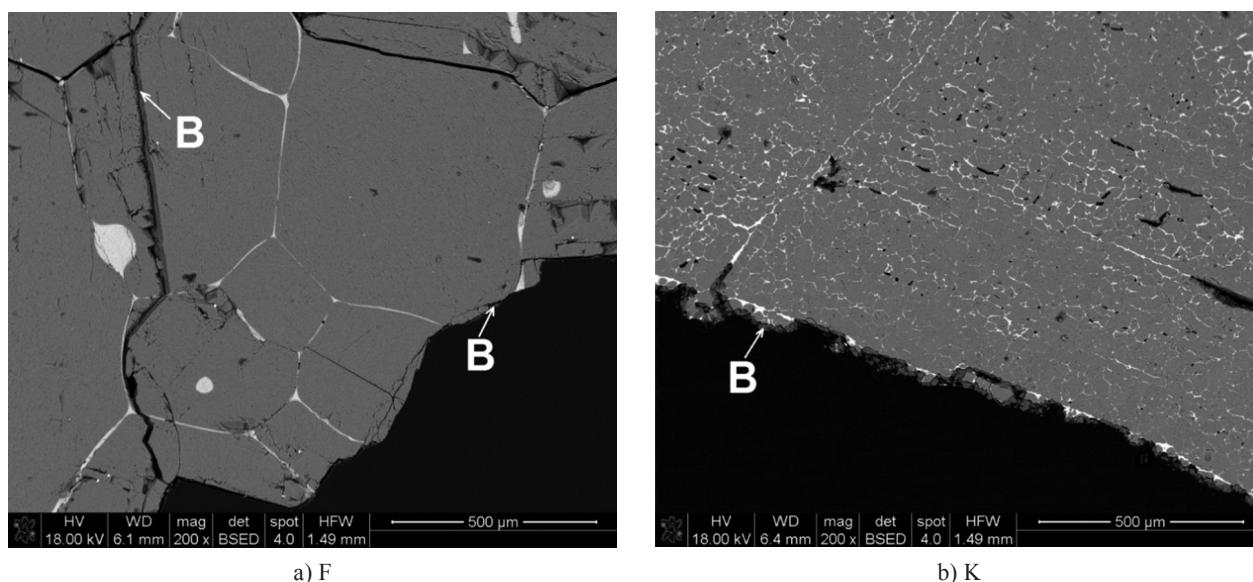
a) F   b) K

Figure 9. BSE-SEM images of the after-hydration magnesia cross-sections a) F, b) K, where 'B' denotes brucite Mg(OH)$_2$, in magnitude: 200 × (C fractions).

phase protects MgO against hydration because it fills intercrystal spaces very tightly and does not allow water to access. Moreover, it is not prone to react with water. There are smaller and larger crystals of MgO visible in the SEM image with their sizes in the range of 30 - 120 µm. The brucite layer (Figure 8b) is mostly present on the surface of magnesia grain with its thickness around 5 µm.

Figures 9 a, b show the after-hydration F and K3 magnesia samples, respectively in the magnitude of 200 ×. It can be observed that the rim of the MgO grain of the F and K3 sample is covered by the thin Mg(OH)$_2$ layer (referred as 'B' in the SEM images); its average size is 15 µm and it is weakly connected with the surface of MgO grain. Moreover, a microstructure of the F sample exhibits an extensive microcrack, on the rim of which

brucite was formed. It can be deduced that presence of the secondary phases like srebrnodolskite (in K3) and merwinite (in F) increases the hydration resistance of magnesia. By 'wetting' the surfaces of MgO crystals and by filling spaces amongst them they constitute a 'natural protector-like' phases, because they do not allow water to penetrates MgO polycrystal.

CONCLUSIONS

The hydrothermal hydration resistance of various magnesia in terms of MgO content as well as the type and the amount of residual impurities has been investigated with the following the most important results:

- Hydration rate observed for the K1 sample, which was characterized by the molar ratio $CaO/SiO_2 > 2$ (containing Ca_2SiO_4 in yhe phase composition), was equal to 70.4 %, and it was around 2, 4 and 8 times higher than hydration rate of K2, F, K3 materials, respectively.

- Srebrnodolskite and magnesium ferrite occurring in K3 magnesia, with the molar ratio $CaO/SiO_2 \gg 2$ and $Al_2O_3/Fe_2O_3 < 1$, seems to be the phases that inhibit MgO hydration considerably. Not regarding ferrites-rich K3 magnesia, fused magnesia exhibits lower tendency to react with water in comparison to K1 and K2 sintered ones.

- Taking all these results into consideration, it can be stated that the nature of magnesia in respect to CaO to SiO_2 molar ratio and the type of thermal treatment (sintered/fused) play one of the most important role next to the granulation in the hydration resistance of magnesia raw materials.

- The analysis of the after-hydration microstructures confirm the literature investigations [9], that the hydration reaction is initiated on the surface of the MgO grain, then it proceeds towards the grain boundaries and continues inside every individual crystal.

Acknowledgments

REFERENCES

1. Rocha S. D., Mansur M. B., Ciminelli V. S. T.: J. Chem. Tech. Biotechnol. *79*, 816 (2004).
2. Amaral L.F., Oliveira I.R., Salomão R., Follini E., Pandofelli V.C.: Ceram. Int. *36*, 1047 (2010).
3. Amaral L.F., Oliveira I.R., Bonadia P., Salomão R, Pandolfelli V.C.: Ceram. Int. *37*, 1537 (2011).
4. Salomão R., Pandolfelli V. C.: Ceram. Int. *34*, 1829 (2008).
5. Khlebnikova Yu., Zhukovskaya A. E., Selivanova A. N.: Ref. Ind. Ceram. *48*, 142 (2007).
6. Salomão R., Pandolfelli V.C.: Cerâmica *54*, 43 (2008).
7. Wojsa J.: *Basic shaped refractories* (in polish), Instytut Szkła, Ceramiki, Materiałów Ogniotrwałych i Budowlanych – Institute of Glass, Ceramics, Refractories and Buildings Materials, Oddział Materiałów Ogniotrwałych w Gliwicach-Department of Refractories in Gliwice, Gliwice 2009.
8. Wojsa J.: Materiały Ceramiczne-Ceramic Materials *61*, 273 (2009).
9. Salomão R., Bittencourt L.R.M., Pandolfelli V.C.: Ceram. Int. *33*, 803 (2007).
10. Ali M.M., Mullick A.K.: Cem.Concr. Res. *28*, 1585 (1998).
11. Sutcu M., Akkurt S., Okur S.: Ceram. Int. *35*, 2571 (2009).
12. Salomão R., Pandolfelli V.C.: Ceram. Int. *37*, 1839 (2011).
13. Van der Merve E.M., Strydom C.A.: J. Therm. Anal. Cal. *84*, 467 (2006).
14. Matabola K.P., Van der Merwe E.M., Strydom C.A., Labuschagne F.J.W.: J. Chem. Tech. Biotechnol. *85*, 1569 (2010).
15. Szczerba J.: *Modified magnesia refractories* (in polish), Ceramika-Ceramics 99 (2007)
16. ASTM C 544-92
17. Galos K., Wyszomirski P.: *Some raw materials of refractory industry-mineralogical and technological characteristics* (in polish), Polski Biuletyn Ceramiczny-Polish Ceramic Bulletin, Polskie Towarzystwo Ceramiczne-Polish Ceramic Society, Kraków 2001.
18. Duran T., Pena P., De Aza S., Gomez-Millan J., Alvarez M., De Aza A. H.: J. Am. Ceram. Soc. *94*, 902 (2011).
19. Todor D.N.: *Thermal analysis of minerals*, Abacus Press, Kent, England 1976.